Flexible and Printed Electronics

PAPER

# Reconfigurable electronic devices enabled by laser-sintered liquid metal nanoparticles

To cite this article: Shanliangzi Liu *et al* 2019 *Flex. Print. Electron.* **4** 015004

View the article online for updates and enhancements.

IOP ebooks™

Bringing you innovative digital publishing with leading voices to create your essential collection of books in STEM research.

Start exploring the collection - download the first chapter of every title for free.

This content was downloaded from IP address 128.102.236.154 on 07/05/2019 at 18:31

Flexible and Printed Electronics

PAPER

# Reconfigurable electronic devices enabled by laser-sintered liquid metal nanoparticles

**Shanliangzi Liu**[1,2], **Michelle C Yuen**[1,2] **and Rebecca Kramer-Bottiglio**[2]

[1] School of Mechanical Engineering, Purdue University, West Lafayette, IN 47907, United States of America
[2] School of Engineering and Applied Science, Yale University, New Haven, CT 06510, United States of America

**E-mail:** rebecca.kramer@yale.edu

**RECEIVED**
23 October 2018

**REVISED**
10 December 2018

**ACCEPTED FOR PUBLICATION**
20 December 2018

**PUBLISHED**
4 February 2019

**Keywords:** eutectic gallium-indium, liquid metal, laser sintering, reconfigurable electronics, flexible and stretchable electronics

## Abstract

Liquid metals are promising conductive materials for creating flexible and stretchable electronic devices. However, methods to pattern liquid metal remain limited in scope: fabrication processes often require substantial manual intervention and the resulting devices are often patterned indelibly into the substrate. In this paper, we demonstrate the creation of electrical traces and components from laser-sintered liquid metal nanoparticles, a digital fabrication approach that creates devices without permanently patterning the materials. As deposited, the liquid metal nanoparticles form a non-conductive film because the conductive liquid metal cores of each particle are surrounded by a non-conductive metal oxide shell. Conductive traces are patterned into the film using an infrared laser to sinter and coalesce the nanoparticles. We demonstrate that we can create resistive and capacitive electrical elements by tailoring the geometry of the laser-sintered patterns. Furthermore, the patterned capacitors can be used to sense the proximity of an object and the patterned resistors can be used in conjunction with analog integrated circuit components to create analog circuits. We show that the fabricated analog circuits can be reconfigured and reused to attain different output responses. The laser processing technique also offers the opportunity to create stretchable conductive traces. We show that compound laser processing can be used to both sinter the nanoparticle film and cut the underlying substrate in the same processing area to achieve in-plane stretching via out-of-plane flexing of liquid metal films.

## 1. Introduction

Flexible and stretchable electronics are essential for soft robotics and wearable systems where electronic devices must be mechanically compatible with highly deformable structures while maintaining functionality [1–5]. Metals that are liquid at or near room temperature have emerged as appealing materials for these applications [6, 7]. Gallium-based liquid metal alloys, such as eutectic gallium–indium, (EGaIn; 75% Ga, 25% In) are inherently conformable conductive materials that are particularly appealing because of their low toxicity [8], low viscosity (2 mPa s) [9], low melting point (15.5 °C), negligible vapor pressure [10] and high electrical conductivity (EGaIn $3.4 \times 10^6$ S m$^{-1}$; copper $5.96 \times 10^7$ S m$^{-1}$) [11]. Gallium-based liquid metals have been used for stretchable and self-healing wires [12–14], stretchable antennas [15–17], actuators [18, 19], electrical interconnects [20, 21], sensors [22–24] and superelastic conductors [25].

Gallium-based liquid metals rapidly form a thin passivating oxide skin (~1–3 nm in ambient environment [26]; ~0.7 nm under vacuum conditions [27, 28]) primarily composed of $Ga_2O_3$ when exposed to an oxygen concentration above 1 ppm [29, 30]. The oxide growth has also been found to be accelerated under elevated temperature [31]. The oxide skin allows liquid metal to adhere to surfaces and to form stable non-spherical shapes [6, 32], but also imparts high surface tension (~624 mN m$^{-1}$ [11, 33]), making the material challenging to process [34]. Existing methods to pattern liquid metals include injection into microchannels [29], masked deposition [35, 36], 3D printing [32, 37], direct writing [38, 39], vacuum-induced patterning [40], embedding into elastomers [41, 42] and subtractive laser

© 2019 IOP Publishing Ltd

ablation [24, 43]. However, these proposed techniques often require premade masks or microchannels formed irrevocably in bulk polymer, making fabrication processes less amenable to rapid prototyping and challenging to automate. In particular, for liquid metal devices that require microchannels or bulk embedding in polymer, the fabrication processes often necessitate manual intervention which renders the process to be inefficient and not scalable, and the devices to be permanent (i.e. non-reconfigurable) becuase the polymer cannot be reformed to create alternate conductive pathways.

Previously, we demonstrated the ability to make liquid metal particle inks and to print them onto various substrates using inkjet [44] and spray printing techniques [45], which are widely known scalable manufacturing methods that are highly compatible with roll-to-roll production [46–49]. The oxide layer on each of the particles insulates them from their neighbors, making the deposited film non-conductive. To coalesce the particles into conductive patterns, the oxide layer must be removed or ruptured, allowing their metal cores to reflow and merge. The simplest method is mechanical sintering—employing pressure to rupture the oxide skin of the particles, without any specialized equipment required [44, 50]. Recently, we showed that a focused laser beam can also be used to coalesce liquid metal cores into electrically conductive patterns. The observed coalescing behavior can be attributed to the rupture of the metal oxide shell due to thermal expansion of the heated liquid metal core [51]. The resistance values of the laser-sintered patterns are significantly affected by laser power. We demonstrated that this method can be used to produce soft multilayer circuits [51] and flexible digital circuits [52] rapidly and efficiently.

In the present work, we utilize the finite resistance of laser-sintered liquid metal particles to program analog circuits by selectively patterning discrete electrical components. Our non-prescriptive approach utilizes scalable deposition and patterning methods suitable for large-area fabrication of arbitrary patterns. We demonstrate that we can use laser sintering to create capacitors and resistors with customized electrical properties. This allows us to create analog sensors and circuits, which we demonstrate by using the sintered capacitor to detect proximity of a finger and by sintering resistors of different values to tune the gains of an opamp circuit, respectively. Furthermore, we show that by encapsulating part of the circuit in polymer, we can selectively reconfigure the fabricated analog circuit by chemically etching away the exposed regions of the circuit, re-printing a layer of liquid metal nanoparticles, and sintering new conductive patterns into the film to attain different output responses. Lastly, we show that we can make stretchable circuits by simply spray printing liquid metal nanoparticles onto polyimide substrates, and then simultaneously laser sintering the particles and cutting tunable kirigami structures. Figure 1 shows a flexible and stretchable device consisting of patterned resistors, capacitors and analog circuits.

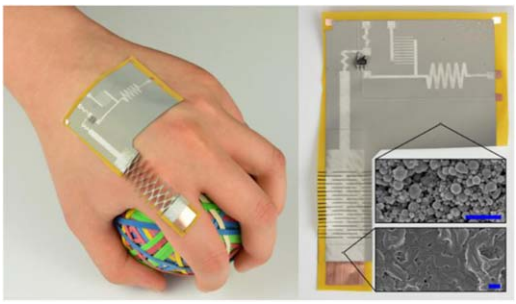

**Figure 1.** Photo of a flexible and stretchable electronic device composed of a laser-sintered liquid metal nanoparticle film deposited onto a flexible printed circuit board (PCB) substrate (copper-clad polyimide film). The laser-sintered patterns (light gray) are used to create conductive traces, resistors, and capacitors between copper traces and integrated circuits. The appendage on the bottom right of the device contains slits to enable stretching of the conductive trace without loss in conductivity. The SEM images show representative areas of the as-printed and laser-sintered particle film. The scale bars are 1 $\mu$m in length. The length of the integrated circuit (black) is 3.15 mm.

## 2. Results and discussion

### 2.1. Analog components

Liquid metal nanoparticle ink was prepared by sonicating bulk eutectic gallium–indium alloy (eGaIn, 75.5% Ga, 24.5% In; 362 $\pm$ 5 mg) in ethanol (4 ml) for 2 h with a tip sonicator (QSonica Q700), as previously presented by Boley *et al* [44]. Ultrasonic waves induce strong shear forces that break up bulk liquid metal into particles. The oxide layer residing on the surface of the liquid metal is continuously broken and rapidly reformed, creating smaller particles. As characterized by Lear *et al* [53] using scanning electron microscopy (SEM), the resulting particle size is 220 $\pm$ 10 nm (mean $\pm$ standard deviation). We etched desired copper patterns into copper-clad polyimide films (Pyralux) and then used a customized spray printer to spray the nanoparticle ink onto the patterned flexible substrate. The spray-printing setup consisted of three micropositioning stages for *x*-, *y*-, and *z*-axis motion (PhysikInstrumente), a compressed air delivery nozzle, and a ink delivery nozzle attached to a syringe pump (883015, Harvard Apparatus). Compressed air (3 psi) was blown over a syringe needle while ink was dispensed at a fixed rate (0.22 ml min$^{-1}$), creating a thin, uniform particle film (20 $\mu$m thickness) on the polyimide substrate. The velocity of the printer stage was 0.7 mm min$^{-1}$. In order to activate the deposited non-conductive nanoparticle film, we used an IR laser (Universal Laser Systems VLS 2.30, 30 W, 10.6 $\mu$m $CO_2$ laser) to sinter the particle film into conductive patterns by scanning a focused laser beam over an area (raster mode, 14% power, 100% speed).

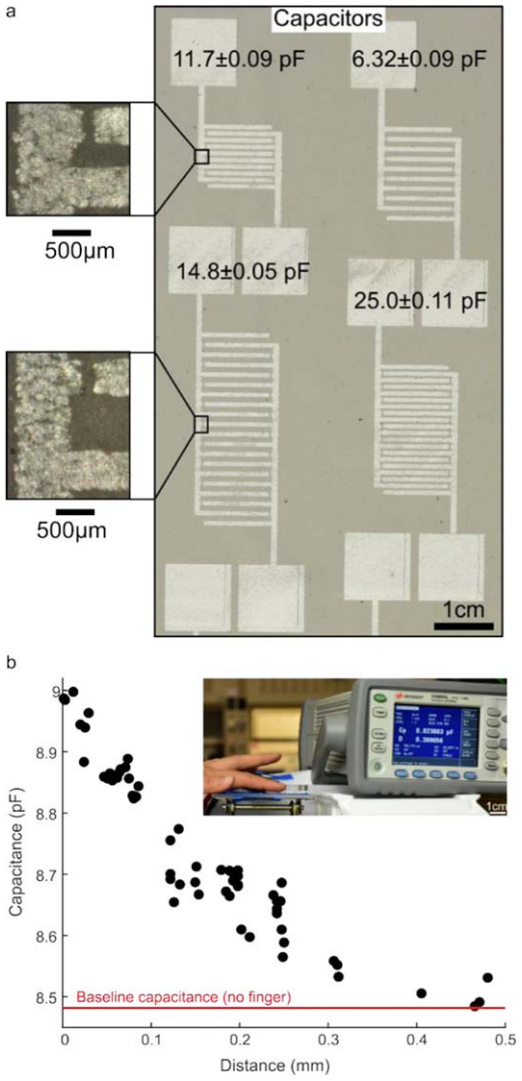


**Figure 2.** Photos and measurements of laser-patterned resistors and capacitors. (a) Interdigitated capacitors where capacitance was modulated by the number and proximity of fingers comprising the device. The mean ± 95% confidence intervals are listed for each device design. The insets show detail views of the patterned capacitors. (b) Demonstration of an interdigitated capacitor being used as a proximity sensor. Each data point was captured by taking a photo of the LCR meter screen and the finger in proximity of the sensor. The red line indicates the mean baseline capacitance of the sensor.

Our previous work demonstrated the ability to coalesce liquid metal nanoparticles into conductive patterns using laser sintering technique and adjusting sheet resistance by tuning laser power [51]. Here, we extend the work beyond simply patterning conductive traces and use laser sintering to create analog electrical components. To demonstrate this, we used fixed laser parameters and varied the geometry of the laser-sintered patterns to attain analog components with different values. Before spray printing and laser sintering, copper electrodes were etched into copper-clad polyimide film to serve as measurement pads. Various laser-sintered capacitors and resistors are shown in figures 2 and 3. The components were sintered using the raster mode in the laser etcher with the long dimension of the component (horizontal direction in figures 2 and 3) oriented parallel to the rastering axis, rather than the scanning direction. This ensured a more repeatable continuous electrical path by avoiding positional error from steps in the scanning direction. In general, the width of a horizontal trace was more consistent along its length as compared to the width of a vertical trace, as seen in the insets of figure 2(a).

Capacitors were sintered in interdigitated capacitor patterns, varying the number of fingers (sintered conductive traces) and the gap between the fingers (unsintered regions) to adjust capacitance values (figure 2(a)). The capacitors were measured using an LCR meter (BK Precision 880) at a 1 kHz interrogation frequency. The mean and 95% confidence intervals of the measured capacitances are reported in figure 2(a). As the number of fingers increase and the gap between the fingers decrease, the capacitance increases.

Additionally, we demonstrated that these planar interdigitated capacitors can be used to sense the proximity of an approaching finger (figure 2(b)). We used an LCR meter (Keysight E4980AL) at a 1 kHz interrogation frequency and 1 V excitation voltage to measure the capacitance while hovering a finger within 1 mm of the surface. The distance between the finger and the surface of the capacitor was measured via optical image analysis where a scale bar of known length was marked onto the support stand and was used to scale the image accordingly. Without a finger nearby, the capacitors had a mean capacitance of 8.48 pF. As the finger approaches the capacitor, the capacitance increases monotonically. When the finger is in contact with the sensor, the capacitance fluctuates at values from approximately 9 to 30 pF due to slight difference in contact conditions (contact area, surface moisture). These preliminary results suggest that laser sintering may be used to create planar capacitive proximity sensors.

Simple resistor patterns with varying trace width (0.25, 0.5, 1, 2, 3, 4 mm) and more intricate serpentine patterns with varying length (one to three segments) were sintered as shown in figures 3(a) and (b), respectively. Despite the feasibility of obtaining patterned traces with distinct resistance values by tuning laser power as indicated previously [51], in this work, we used fixed laser processing parameters for all samples and only varied pattern geometries. We first measured the sheet resistance of sintered dogbone patterns on spray-printed nanoparticle films, all processed with the same laser parameters (14% power, 100% speed) using the four-probe resistance measurement method. The sheet resistance of the sintered patterns was relatively consistent (1.94 ± 0.15Ω/sq, mean ±95% confidence interval, 12 measurements) across samples. Using this mean sheet resistance value, we calculated the expected resistance of the various resistors with different geometries and compared it to the measured values (figures 3(d), (e)). The calculated values tended

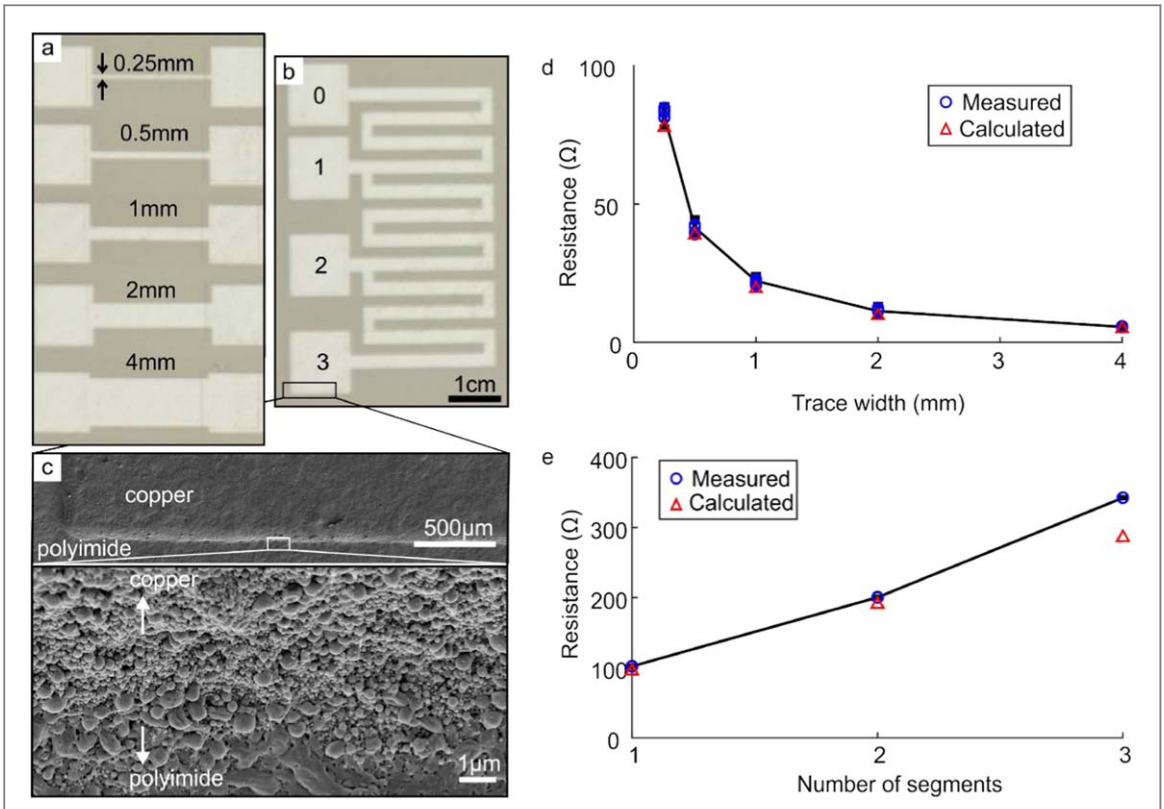


**Figure 3.** (a) Simple resistor patterns with varying trace width (0.25, 0.5, 1, 2, 3, 4 mm). (b) Serpentine resistor patterns with varying length (one to three segments). (c) SEM images of the interface between the sintered trace and a copper pad. (d)–(e) Resistance values of the components shown in (a)–(b) as measured and as calculated from sheet resistance values. The error bars represent 95% confidence intervals of the measured resistance and capacitance values.

to underestimate the measured value by ~5%–15%. We hypothesize that this is primarily due to contact resistance between the laser-sintered trace and the copper measurement pad.

While the particles on top of the copper pads and the polyimide substrate form fully-coalesced networks, the particles connecting them are not fully-coalesced which contributes to an increased resistance, as evidenced by the larger but discontinuous particles seen at the edge of the copper pad in figure 3(c). We hypothesize that this is due to the steep, cliff-like edge of the copper pad traversed by the nanoparticle film. Since the spray printing distributes nanoparticles in a cone rather than a downward jet, nanoparticles are deposited on all surfaces regardless of their angle. In contrast, laser sintering acts only in a downward direction. Thus, the particles residing on the angled edge of the copper pad are sintered with less energy per unit area, resulting in a partially coalesced network that only tenuously spans the region between the sintered pattern on the polyimide film and on the copper pad. Future work can mitigate this issue by using thermal evaporation or other approaches to deposit thinner copper layers onto the substrate. These improvements would enable creation of patterns with resistance values that more closely match the theoretical calculations based on constant sheet resistance and the pattern geometry.

### 2.2. Analog circuits

We utilized the ability to pattern conductive traces at specific resistances to create analog circuits. Here, we used an operational amplifier (opamp) integrated circuit (MCP6001, Microchip Technology) to create a non-inverting amplifying circuit with tunable gains using laser-sintered resistors (figure 4(a)). The opamp was first soldered to the copper traces of an IC breakout substrate. The liquid metal ink was then deposited and patterned onto the substrate, over copper traces where necessary (ex. $R_1$ lies on top of the copper trace leading from the IC to $V_{out}$). Here, the sprayed film was deposited to a thickness of 30 $\mu$m to better ensure electrical isolation between the sintered liquid metal trace and the underlying copper trace. The nominal output of the non-inverting amplifier circuit is the input voltage signal multiplied by the gain, calculated as $\text{Gain} = V_{out}/V_{in} = 1 + R_1/R_2$. We varied the dimensions of the sintered traces to obtain different resistance values and nominal gains, as tabulated in figure 4(b). To determine the actual gain of the circuits, we supplied a 50 mVpp sinusoidal signal with a 50 mV offset and measured the output signal with an oscilloscope. Representative responses are shown in figure 4(c). The mean measured gains are listed in the table in figure 4(b).

Although the output signal of the opamps clearly demonstrate voltage gain, the measured gain is less than that of the nominal value. We hypothesize

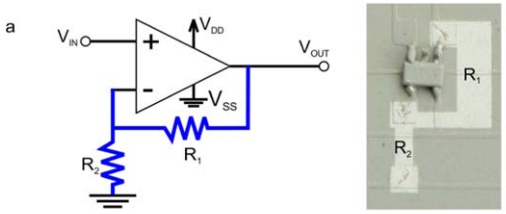


b

| $R_1$ | $R_2$ | Nominal Gain | Actual Gain |
|---|---|---|---|
| 46.4 Ω | 14.8 Ω | 4.14 | 3.33 |
| 32.2 Ω | 13.2 Ω | 3.44 | 2.78 |
| 20.3 Ω | 10.5 Ω | 2.93 | 2.04 |

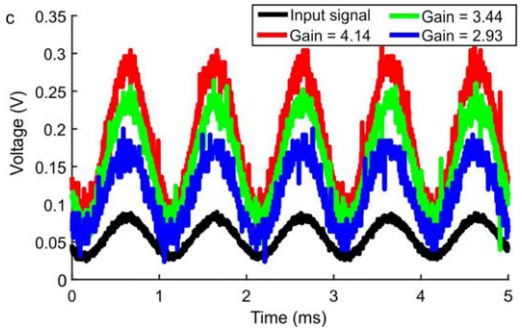


**Figure 4.** Design and characterization of opamp circuits with gain programmed by laser-sintered resistive traces. (a) Schematic of the implemented circuit. The image on the right shows the laser-sintered liquid metal nanoparticle film deposited over an opamp IC soldered to copper traces on a polyimide substrate. The length of the IC is 3.15 mm. (b) Table of resistance values, nominal gain, and actual gain of circuits with three different gains. (c) Plot of the input and output voltage signals.

that this is due to slightly conductive (~400 kΩ) connections between the coalesced liquid metal patterns as they are sintered over copper traces, i.e. between $R_1$ and the $V_{DD}$ copper trace. As demonstrated in our previous work [51], due to exposure to high temperature, the uncoalesced particles at the bottom of the sintered film are likely to become conductive because (1) gallium oxides become semiconductive at high temperatures [54, 55], and (2) particles coarsen and fuse together at high temperatures, as seen from thermal treatment of solid metal particles [56, 57]. Therefore, the thermally treated but uncoalesced particles become electrically connected to the underlying copper traces. The effective sintering depth (the distance at which uncoalesced particles become conductive) is dependent on laser parameters. Future work will aim to identify the appropriate laser sintering parameters so that conductive patterns may be sintered to a specific depth, without inadvertently connecting to underlying copper traces. Work in this area will also aid in repeatably fabricating the conductive interface between the liquid metal film and a copper pad. While the contact resistance is not as significant of an issue for logic devices, in an analog circuit, contact resistance may not be so easily discounted.

Alongside the resistors (figures 3(a)–(b)) shown here, capacitive components (figure 2(a)) may also be laser-sintered to create more complex analog circuits, in particular, with the addition of other analog components or ICs. Furthermore, while this device is a two-layer electronic circuit, the concept of spray printing and laser sintering over existing conductive traces may be extended to create multilayer circuits.

### 2.3. Circuit reconfigurability

Unlike traditional electronic circuits, the demonstrated liquid metal patterned analog circuits are reusable. They can be rapidly reconfigured multiple times to achieve different output responses via the process of chemical etching, re-printing and re-patterning. Figure 5 shows the fabrication process of an reconfigurable analog circuit.

The substrate was first prepared prior to deposition of liquid metal. Flexible copper-clad polyimide film (Pyralux, Adafruit) was covered with Kapton tape as an etching mask. The Kapton tape was cut to mask the copper pattern using an IR laser (Universal Laser Systems VLS 2.30, 30 W, 10.6 $\mu$m $CO_2$ laser; vector mode, 25% power, 20% speed). The undesired copper was then etched off the polyimide film using hydrochloric acid and hydrogen peroxide. Standard electrical components (integrated circuits (ICs)) were soldered to the copper traces (figure 5(a)). Small pieces of masking tape were applied to each of the ICs and along the edges of the substrate to mask the components and copper interface pads, respectively (figure 5(b)). The nanoparticle ink was then sprayed onto the circuit using a customized spray printer (figure 5(c)). Next, the laser was used to sinter the particle film into conductive patterns by scanning a focused laser beam over an area (raster mode, 14% power, 100% speed). As observed in figure 5(d), the sintered, conductive traces appear white. The SEM images in figure 1 show the intact particles in the unsintered regions and the coalesced morphology of the sintered region.

Because the oxide skin of liquid metal is amphoteric, it can be removed by exposure to hydrochloric acid (HCl, pH $<$ 3) [58] or sodium hydroxide (NaOH, pH $>$ 10) [59]. In the absence of the oxide skin, liquid metal that adheres to the surfaces can bead up due to high surface tension of the bare metal [11]. Therefore, chemical treatment can be used to remove existing liquid metal films, allowing the device to be reconfigured. Here, we used NaOH due to its proven fast dissolution of oxide compared to HCl [59].

In order to selectively reconfigure the device, part of the circuit was encapsulated by casting a thin layer of PDMS (Sylgard 184, Dow Corning) over the nanoparticle film, appearing as a dark gray region (figure 5(e)). After the PDMS cured, the circuit was rinsed with 1.0 M sodium hydroxide (NaOH) for a few seconds. As shown in figure 5(f), the exposed particle film was etched away, while the encapsulated region was protected by the PDMS. The circuit was then

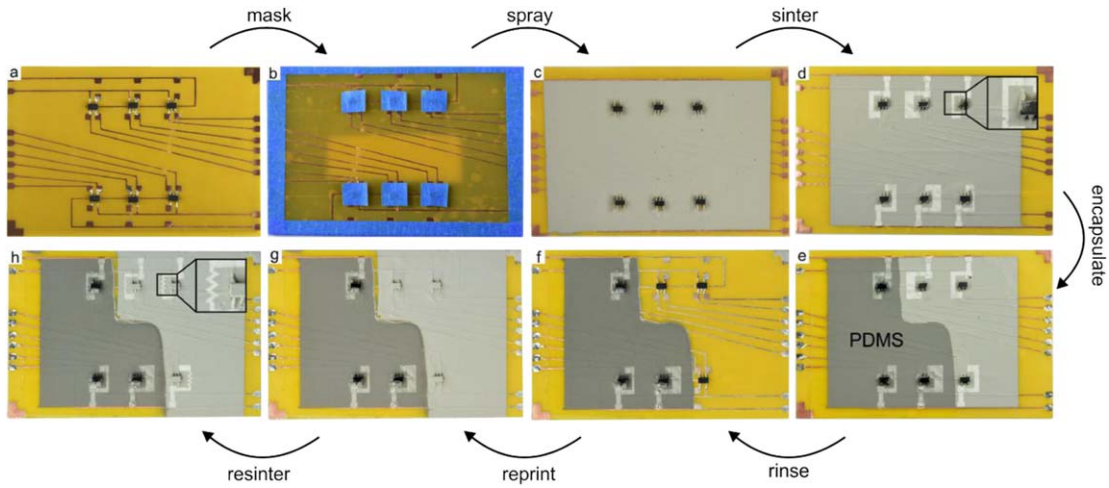


**Figure 5.** Fabrication process of analog circuits. (a) Flexible PCB on a copper-clad polyimide film (Pyralux) with integrated circuit (IC) components soldered to copper traces. (b) Tape applied to mask ICs before spray printing. (c) Spray-printed liquid metal nanoparticle film. (d) Analog circuits created by laser sintering liquid metal traces patterned to interface with the ICs. (e) Partial encapsulation of the device using silicone elastomer (polydimethylsiloxane (PDMS)). (f) Unencapsulated region exposed after rinsing with NaOH. (g) Re-spray-printed liquid metal nanoparticle film. (h) Final analog circuit device with particle film re-sintered into zigzag patterns. The steps shown in (f)–(h) may be repeated to reconfigure the circuit multiple times. The close-up views in (d) and (h) highlight the sintered traces with different geometries. The length of the IC is 3.15 mm.

wiped with NaOH using a paper towel rinsed with water, and dried. Finally, the partially etched circuit was reprinted (figure 5(g)) and re-sintered into different geometries (zigzag patterns, figure 5(h)). This selective reconfiguration sequence can be repeated multiple times to reconfigure the circuit to attain different output responses. Additionally, since the PDMS does not bond to the Pyralux substrate, the PDMS encapsulation layer may be peeled away to expose the liquid metal film underneath for full device reconfiguration. The PDMS encapsulation also serves to maintain the integrity of the film by preventing cracking and disruption of both the sintered and unsintered regions for more stable electrical properties as the circuit is bent or flexed.

### 2.4. Stretchable circuits

Taking inspiration from kirigami—the art of paper cutting—we created stretchable conductive traces by cutting through the polyimide substrate after sintering the liquid metal film. Researchers have shown that modulating the geometry of the cutting pattern can yield substrates with different degrees of stretchability [60, 61], and have begun to create stretchable conductors using this approach [62, 63]. The specimens shown in figures 6(a)–(d) consist of copper electrodes on either end of a polyimide substrate with a large sintered region connecting the electrodes. Overlapping slits were cut through the polyimide substrate underneath the sintered region to enable stretching. To tune the stretchability of the traces, we varied the horizontal distance between parallel vertical slits (i.e. slit density) (1 mm; 2 mm) and the vertical gap distance (1 mm; 2 mm) between collinear slits. The probe interface shown in figure 6(c) shows a droplet of bulk liquid metal enhancing the electrical contact between the probe and the sintered pattern. The SEM image in figure 6(d) shows the coalescence of particles around the slit cut through the polyimide film. Because both the sintering and kirigami processes can be performed in the same laser patterning step, stretchable circuits with tunable electrical and mechanical properties can be rapidly manufactured.

We characterized the stretchable circuits by recording the resistance between the copper electrodes as strain was applied cyclically (ex. 0%, 10%, 0%, 20%, etc.) (figure 6(e)). The normalized change in resistance ($\Delta R/R_0 = (R - R_0)/R_0$) effectively does not change with applied strain until electrical and/or mechanical failure suddenly occurs. We classified electrical failure as a normalized change in resistance >0.5. The 2 × 2 (figure 6(a)) and 2 × 1 (figure 6(b)) designs exhibited near-simultaneous (within 10% strain) mechanical and electrical failure between 50% and 60% strain. Increasing the slit density (1 × 2 (Figure 6(c)), 1 × 1 (figure 6(d))) allowed the devices to stretch further and to electrically fail at strains significantly less than the yield strain for mechanical failure. After reaching electrical failure, we restarted the strain increment at 0% strain and repeated the same test (figure 6(f)). After the first electrical failure, the resistance did not return to its initial value when the strain was released; the resistance of the sintered pattern was irreversibly increased. During the second strain sequence, electrical failure occurred at the same strain value. These results indicate that laser-sintered liquid metal films deposited onto polymer substrates may be used as stretchable interconnects where strain (up to a limit) does not

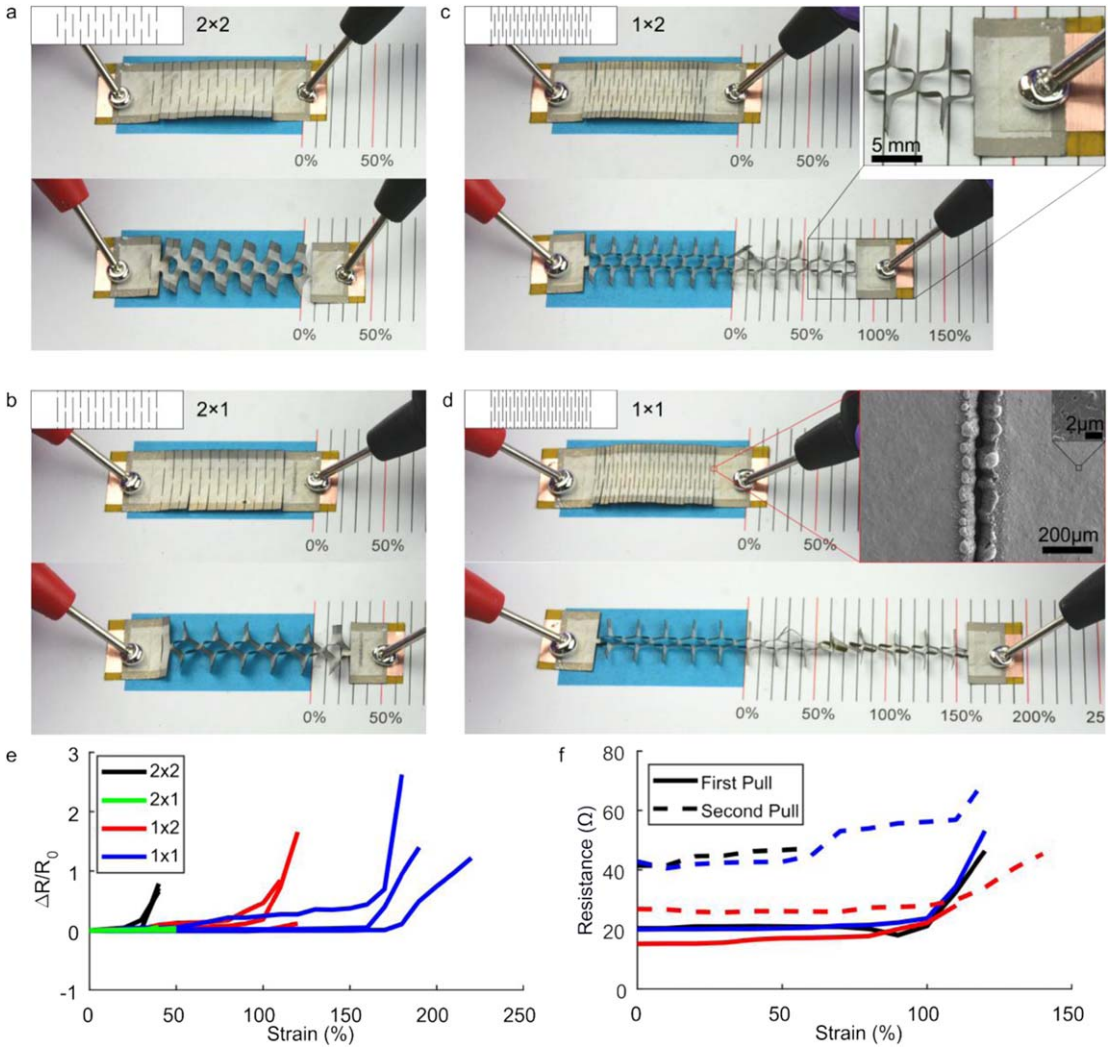


**Figure 6.** Stretchable conductive liquid metal films enabled by kirigami. The four slit patterns are shown in (a)–(d). In each subfigure, the top photo shows the unstretched state of the sample, with the inset being the slit pattern labeled as (distance between slits) × (gap between collinear slits) in mm. The bottom photo shows the maximum strain achieved prior to electrical and/or mechanical failure. The spacing between each line is 3 mm (10% strain). The probe interface shown in (c) shows a droplet of bulk liquid metal enhancing the electrical contact between the probe and the sintered pattern. The SEM image in (d) shows the coalescence of particles around the slit cut through the polyimide film. (e) Plots of the normalized resistance as strain was applied in 10% increments from 0% strain to electrical and/or mechanical failure. Three specimens of each slit pattern were measured. (f) Plot of the resistance of three samples cut with a 1 × 2 slit pattern shown in (c). The solid line corresponds to the first strain sequence wherein strain was applied incrementally until there was a significant change in the measured resistance (electrical failure. The strain sequence was then re-initiated at 0% strain and the experiment was repeated (dashed line).

affect the conductivity of the trace. In contrast, the resistance of interconnects fabricated on inherently stretchable substrates would change as strain is applied due to a change in the geometry of the trace or cracking of the liquid metal nanoparticle film. Future work in this area will investigate alternate kirigami designs to attain different levels of stretch and the effects of repeated cycles of stretching on electromechanical behavior of the interconnect.

## 3. Conclusion

Laser sintering of liquid metal nanoparticle films enables the rapid fabrication of arbitrary conductive patterns. In this paper, we demonstrated that this method may be used to create analog electrical components, hybrid flexible circuits, and stretchable circuits. We explored the fabrication of resistors and capacitors where electrical properties were modulated by the geometric design of the laser sintering pattern. Using these elemental components, we demonstrated an opamp circuit by sintering resistors of different values to tune the gains, and a proximity sensor to detect an approaching finger. We showed that these circuits may be selectively reconfigured via encapsulation, chemical etching, and re-patterning. Finally, we discussed how the materials and methods used here (i.e. selective laser processing of conductive films on flexible polymer substrates) can be leveraged to create stretchable conductive circuits using kirigami methods.

Future work will further characterize the applications demonstrated here, translate the laser sintering approach to inherently stretchable substrates, and to combine the various methods presented here to create more complex, flexible, and stretchable electronic devices. Another area of future work is to create more sophisticated components, namely those with semiconductive materials. Because the oxide skin has semiconductive properties, further investigation into tuning the electrical properties of the nanoparticles and designing more intricate methods of patterning the liquid metal ink may yield liquid metal-enabled diodes and transistors.

## Acknowledgments

Shanliangzi Liu and Michelle C Yuen contributed equally to this work. The authors would like to thank Jennifer C Case and Edward L White for their comments and insight on this project. This work was supported by the National Science Foundation (CAREER Award 1454284). Michelle C Yuen was supported by a National Science Foundation Graduate Research Fellowship (Grant DGE-1333468).

## ORCID iDs

Shanliangzi Liu https://orcid.org/0000-0002-6362-801X

## References

[1] Lu N and Kim D H 2013 *Soft Robot.* **1** 53–62
[2] Rich S I, Wood R J and Majidi C 2018 *Nat. Electron.* **1** 102–12
[3] Manti M, Cacucciolo V and Cianchetti M 2016 *IEEE Robot. Autom. Mag.* **23** 93–106
[4] Stoppa M and Chiolerio A 2014 *Sensors* **14** 11957–92
[5] Liu Y, Pharr M and Salvatore G A 2017 *ACS Nano* **11** 9614–35
[6] Dickey M D 2017 *Adv. Mater.* **29** 1606425
[7] Wang Q, Yu Y and Liu J 2017 *Adv. Eng. Mater.* **20** 1700781
[8] Hallfors N, Khan A, D Dickey M and Marion Taylor A 2013 *Lab Chip* **13** 522–6
[9] Spells K E 1936 *Proc. Phys. Soc.* **48** 299
[10] Geiger F, Busse C A and Loehrke R I 1987 *Int. J. Thermophys.* **8** 425–36
[11] Zrnic D and Swatik D S 1969 *J. Less-Common Met.* **18** 67–8
[12] Zhu S, So J H, Mays R, Desai S, Barnes W R, Pourdeyhimi B and Dickey M D 2013 *Adv. Funct. Mater.* **23** 2308–14
[13] Park J, Wang S, Li M, Ahn C, Hyun J K, Kim D S, Kim D K, Rogers J A, Huang Y and Jeon S 2012 *Nat. Commun.* **3** 916
[14] Palleau E, Reece S, Desai S C, Smith M E and Dickey M D 2013 *Adv. Mater.* **25** 1589–92
[15] Zandvakili M, Honari M M, Mousavi P and Sameoto D 2017 *Adv. Mater. Technol.* **2** 1700144
[16] Kubo M, Li X, Kim C, Hashimoto M, Wiley B J, Ham D and Whitesides G M 2010 *Adv. Mater.* **22** 2749–52
[17] Qusba A, RamRakhyani A K, So J H, Hayes G J, Dickey M D and Lazzi G 2014 *IEEE Sens. J.* **14** 1074–80
[18] Russell L, Wissman J and Majidi C 2017 *Appl. Phys. Lett.* **111** 254101
[19] Tang S-Y, Sivan V, Petersen P, Zhang W, Morrison P D, Kalantar-Zadeh K, Mitchell A and Khoshmanesh K 2014 *Adv. Funct. Mater.* **24** 5851–8
[20] Hirsch A, Michaud H O, Gerratt A P, de Mulatier S and Lacour S P 2016 *Adv. Mater.* **28** 4507–12
[21] Yoon J, Hong S Y, Lim Y, Lee S-J, Zi G and Ha J S 2014 *Adv. Mater.* **26** 6580–6
[22] Park Y L, Majidi C, Kramer R, Bérard P and Wood R J 2010 *J. Micromech. Microeng.* **20** 125029
[23] Sahlberg A, Nilsson F, Berglund A, Nguyen H, Hjort K and Jeong S H 2018 *Adv. Mater. Technol.* **3** 1700330
[24] Pan C, Kumar K, Li J, Markvicka E J, Herman P R and Majidi C 2018 *Adv. Mater.* **30** 1706937
[25] Wang J, Cai G, Li S, Gao D, Xiong J and Lee P S 2018 *Adv. Mater.* **0** 1706157
[26] Scharmann F, Cherkashinin G, Breternitz V, Knedlik C, Hartung G, Weber T and Schaefer J A 2004 *Surf. Interface Anal.* **36** 981–5
[27] Regan M J, Tostmann H, Pershan P S, Magnussen O M, DiMasi E, Ocko B M and Deutsch M 1997 *Phys. Rev.* B **55** 10786–90
[28] Cademartiri L *et al* 2012 *J. Phys. Chem.* C **116** 10848–60
[29] Dickey M D, Chiechi R C, Larsen R J, Weiss E A, Weitz D A and Whitesides G M 2008 *Adv. Funct. Mater.* **18** 1097–104
[30] Liu T, Sen P and Kim C J 2012 *J. Microelectromech. Syst.* **21** 443–50
[31] Cutinho J, Chang B S, Oyola-Reynoso S, Chen J, Akhter S S, Tevis I D, Bello N J, Martin A, Foster M C and Thuo M M 2018 *ACS Nano* **12** 4744–53
[32] Ladd C, So J H, Muth J and Dickey M D 2013 *Adv. Mater.* **25** 5081–5
[33] Larsen R J, Dickey M D, Whitesides G M and Weitz D A 2009 *J. Rheol.* **53** 1305–26
[34] Khondoker M A H and Sameoto D 2016 *Smart Mater. Struct.* **25** 093001
[35] Kramer R K, Majidi C and Wood R J 2013 *Adv. Funct. Mater.* **23** 5292–6
[36] Gozen B A, Tabatabai A, Ozdoganlar O B and Majidi C 2014 *Adv. Mater.* **26** 5211–6
[37] Daalkhaijav U, Yirmibesoglu O D, Walker S and Mengüç Y 2018 *Adv. Mater. Technol.* **3** 1700351
[38] Boley J W, White E L, Chiu G T C and Kramer R K 2014 *Adv. Funct. Mater.* **24** 3501–7
[39] Gao Y, Li H and Liu J 2012 *PLoS ONE* **7** e45485
[40] Lin Y, Gordon O, Rashed Khan M, Vasquez N, Genzer J and D Dickey M 2017 *Lab Chip* **17** 3043–50
[41] Kazem N, Hellebrekers T and Majidi C 2017 *Adv. Mater.* **29** 1605985
[42] Fassler A and Majidi C 2015 *Adv. Mater.* **27** 1928–32
[43] Lu T, Markvicka E J, Jin Y and Majidi C 2017 *ACS Appl. Mater. Interfaces* **9** 22055–62
[44] Boley J W, White E L and Kramer R K 2015 *Adv. Mater.* **27** 2355–60
[45] Mohammed M G and Kramer R 2017 *Adv. Mater.* **29** 1604965
[46] Ko S H, Pan H, Grigoropoulos C P, Luscombe C K, Fréchet J M J and Poulikakos D 2007 *Nanotechnology* **18** 345202
[47] Li Z, Klein T R, Kim D H, Yang M, Berry J J, Hest M F A M V and Zhu K 2018 *Nat. Rev. Mater.* **3** 18017
[48] Angmo D, Larsen-Olsen T T, Jørgensen M, Søndergaard R R and Krebs F C 2013 *Adv. Energy Mater.* **3** 172–5
[49] Morton S W, Herlihy K P, Shopsowitz K E, Deng J, Chu K S, Bowerman C J, DeSimone J M and Hammond P T 2013 *Adv. Mater.* **25** 4707–13
[50] Lin Y, Cooper C, Wang M, Adams J J, Genzer J and Dickey M D 2015 *Small* **11** 6397–403
[51] Liu S, Yuen M, White E L, Boley J W, Deng B, Cheng G J and Kramer-Bottiglio R 2018 *ACS Appl. Mater. Interfaces* **10** 28232–41
[52] White E L, Case J C and Kramer R K 2017 *2017 IEEE SENSORS* pp 1–3
[53] Lear T R, Hyun S H, Boley J W, White E L, Thompson D H and Kramer R K 2017 *Extreme Mech. Lett.* **13** 126–34
[54] Ortiz A, Alonso J C, Andrade E and Urbiola C 2001 *J. Electrochem. Soc.* **148** F26–9

[55] Basharat S, Carmalt C J, King S J, Peters E S and Tocher D A 2004 *Dalton Trans.* 3475–80
[56] Ermak O, Zenou M, Toker G B, Ankri J, Shacham-Diamand Y and Kotler Z 2016 *Nanotechnology* **27** 385201
[57] Pan H, Ko S H and Grigoropoulos C P 2008 *J. Heat Transfer* **130** 092404
[58] Doudrick K, Liu S, Mutunga E M, Klein K L, Damle V, Varanasi K K and Rykaczewski K 2014 *Langmuir* **30** 6867–77
[59] Bilodeau R A, Zemlyanov D Y and Kramer R K 2017 *Adv. Mater. Interfaces* **4** 1600913
[60] Rafsanjani A, Zhang Y, Liu B, Rubinstein S M and Bertoldi K 2018 *Sci. Robot.* **3** eaar7555
[61] Tang Y, Lin G, Yang S, Yi Y K, Kamien R D and Yin J 2016 *Adv. Mater.* **29** 1604262
[62] Blees M K *et al* 2015 *Nature* **524** 204–7
[63] Hwang D G and Bartlett M D 2018 *Sci. Rep.* **8** 3378